JOURNAL OF SOLID STATE CHEMISTRY 41, 195–204 (1982)

Phase Diagram of Pseudobinary CrB–MnB and MnB–FeB Systems: Crystal Structure of the Low-Temperature Modification of FeB

TADAHITO KANAIZUKA

Department of Chemistry, Faculty of Science, Kyoto University, Kyoto, Japan

Received July 14, 1981; in revised form October 20, 1981

Phase diagrams of pseudobinary CrB–MnB and MnB–FeB systems were studied in the temperature range from 600 up to 2400°C. In the $Cr_xMn_{1-x}B$ system, both the CrB and the FeB type structures could be obtained as temperature modifications in the composition range between $x = 0.35$ and 0.80. Low-temperature modifications were obtained, i.e., the MoB type structure for CrB and the mixed stacking variants of the CrB and the FeB type structures for MnB and FeB. A model structure of the low-temperature modification of FeB was proposed.

Introduction

The structural relation between the CrB and the FeB type structures has been investigated on many rare earth silicides, germanides, rare earth–platinum, rare earth–nickel alloys (*1–4*), and alkaline metal–noble metal compounds (*5*). Investigation on transition metal monoborides, on the other hand, is rather meager (*6*) in spite of the names of the structural types being given to these compounds. This may be due to the difficulty of sample preparation because of slow diffusion rate of constituents even at high temperature and volatility at high temperature.

The FeB and the CrB type structures are geometrically closely related to each other. One can obtain the FeB type structure from the CrB type and vice versa by slicing the structure into identical structure slabs and displacing these slabs in a particular manner. The concept of unit cell twinning of the hexagonal and the cubic close-packed structure proposed by Andersson and Hyde (*7*) and Hyde *et al.* (*8*) made it easier to understand the structural relation between them, and suggested the possibility of various intermediate structures or ordered intergrowth of them. CrB has been reported to crystallize with the CrB type structure, and MnB and FeB to crystallize with the FeB type structure at high temperature. No phase diagrams for the system CrB–MnB or MnB–FeB have been found in the literature, although a number of investigators have prepared transition metal monoborides to study physical properties, especially magnetism (*9, 10*) and magnetovolume effects (*11, 12*). In the present paper, the phase diagram and crystallographic aspects of the pseudobinary systems CrB–MnB and MnB–FeB are reported. A model structure for the low-temperature modification of FeB, which was suggested to be the defect structure of the normal FeB type structure by Fruchart (*13*), is proposed as an intermediate structure of the CrB and

0022-4596/82/020195-10$02.00/0

the FeB type structure. Moreover MnB and CrB are also shown to have low-temperature modifications.

Experimental

The samples were prepared by direct reaction from metals and boron of high purity (99.9 and 99.5%, respectively). Chromium and iron were supplied in powder form, and their particle sizes were less than 300 mesh. As manganese is easily oxidized in air, it was crushed from blocks just before use. Boron was also crushed into a fine powder in an alumina mortar. Elements in powder form were mixed in a certain ratio, with addition of several percent excess boron to avoid the formation of metal-rich compounds, and they were pelletted at 3 ton/cm^2 prior to reaction. To make samples homogeneous, each sample was heated previously at a temperature lower than the prescribed temperature. The reaction was made in evacuated silica tubes up to 1250°C in electroresistance furnaces. Temperature was measured by a calibrated Pt · Pt-13%Rh thermocouple. In the case of preparing the low-temperature modification of FeB, a porous alumina tube 2 cm thick was used as a temperature buffer and the temperature fluctuation could be suppressed within a few degrees.

At a temperature higher than 1250°C, a high-pressure sample-synthesizing apparatus (piston-cylinder type), shown in Fig. 1, was used. Boron nitride is a good material for the crucible. No reaction between the crucible and the samples was observed even at the highest temperature of the operations. Another reason to use the apparatus is that the pressure-sealed crucible prevents the elements from evaporating. The dimensions of the sample chamber were limited to 3.5 mm diameter and 4 mm length to avoid inhomogeneity of the temperature. Temperature measurement was carried out using a W-5%Re · W-26%Re thermocouple. The temperature difference between the sample chamber and the thermocouple was calibrated prior to the operation. The reproducibility of the temperature control was quite good. As a temperature standard, the melting points of iron and niobium were adopted. Though the experiments were carried out under a pressure of 10 kb, no pressure correction was made, because no appreciable difference was detected between the samples treated at 10 and at 15 kb. A smooth connection of phase diagrams obtained from the experiment above 1250°C and below 1250°C supports the justifiability of this treatment.

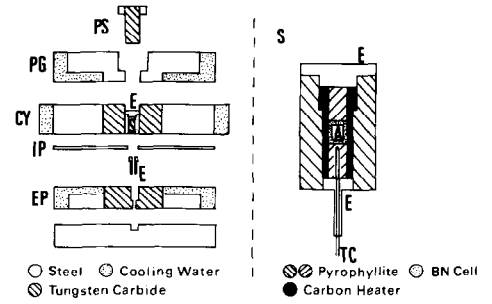

FIG. 1. High-pressure apparatus used for sample preparation above 1250°C. PS, piston; PG, piston guide; CY, cylinder; IP, insulating paper; EP; end plate; E, electrode for heater; TC, thermocouple; A, sample chamber.

X-ray powder diffraction patterns were taken with a Rota-Unit diffractometer (Rigaku) using Cu$K\alpha$ and Cr$K\alpha$ radiation with a Ni and V filter, respectively, in order to analyze the crystal structure of the samples.

Results and Discussion

The phase diagram obtained in this work is shown in Fig. 2. As mentioned above, the samples prepared below 1250°C were annealed in silica tubes, and quenched from the annealing temperature into iced water; the samples above 1250°C were annealed in boron nitride crucibles by using a high-

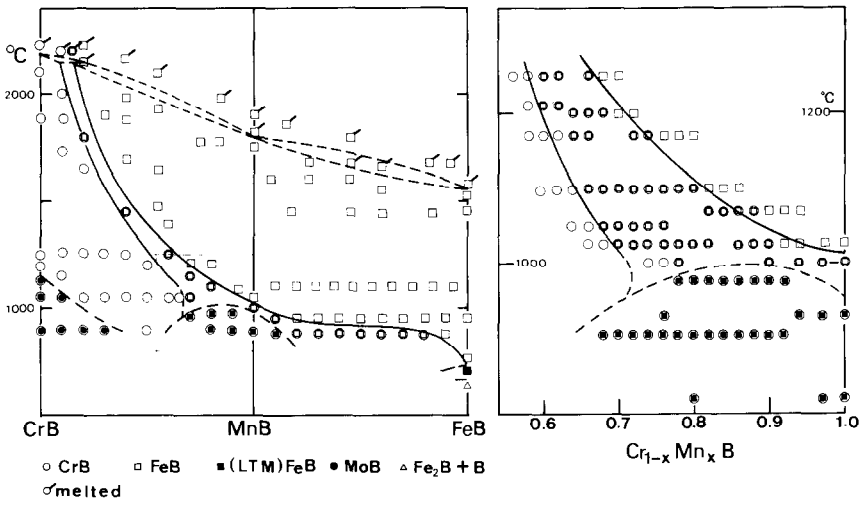

FIG. 2. Phase diagram of pseudobinary CrB–MnB system and MnB–FeB system. The detail of a part enclosed by the dotted line in the left figure is shown in the right. Overlapped two kinds of marks represent two phases.

pressure–high-temperature apparatus and quenched at a rate of −400°C/sec to room temperature by turning off the heater current.

Melted samples were judged from the look of the surface of the samples. When the sample had melted, the surface was smooth and the separation from the crucible was very easy. The effect of melting also appeared on the X-ray diffraction patterns. If the sample had melted, the X-ray powder pattern was rather broad except for the end members (CrB, MnB, and FeB).

Here let us briefly review the known crystal structures appearing in these systems in order to aid understanding of this paper. The pseudobinary CrB–MnB system has different structure types at both ends of the phase diagram. CrB has the CrB type structure which is orthorhombic with space group *Cmcm* (D_{2h}^{17}), and MnB has the FeB type structure which is orthorhombic with space group *Pbnm* (D_{2h}^{16}). As shown in Fig. 3, both structures are closely related and are characterized by trigonal prism rows sharing their rectangular faces and infinite zigzag chains of borons running through the rectangular faces of the trigonal prisms. The difference of the structures depends only on how these rows are arranged. Another view of the structural relation between these two structures was given by the model of unit cell twinnings (*14–16*). Both of the structures are derived by successive unit cell twinning of close-packed structures. The CrB type structure is interpreted as a successive unit cell twinning of a cubic close-packed structure and the FeB type structure as that of a hexagonal close-packed structure.

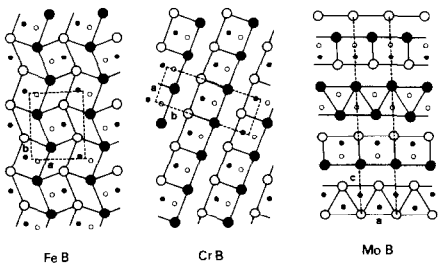

FIG. 3. Crystal structures of the FeB, CrB, and MoB type. Dotted lines indicate the unit cells of the structures. Small circles represent boron atoms and large circles represent metal atoms; open and closed circles are at a height of ¼ and ¾, respectively.

Two other structures were observed in the low-temperature modification phases. Near the end member CrB, the MoB type structure appeared, and the intermediate intergrowth structure of the CrB and the FeB type (isomorphous to (LTM)FeB) was observed in the range near MnB. The MoB type structure is of tetragonal symmetry with space group $I4/amd$ (D_{4h}^{19}) as shown in Fig. 3. The unit cell is twice as large as that of the CrB type structure. If half of the MoB type unit cell is transposed $\frac{1}{2}\ \frac{1}{2}\ 0$ (referred to the tetragonal axes), one can obtain the CrB type structure. So the face of the trigonal prism parallel to the boron chain must be square in the tetragonal MoB type structure.

The low-temperature modification at FeB and near MnB will be discussed later.

The different phase regions observed are described in more detail in the sections which follow.

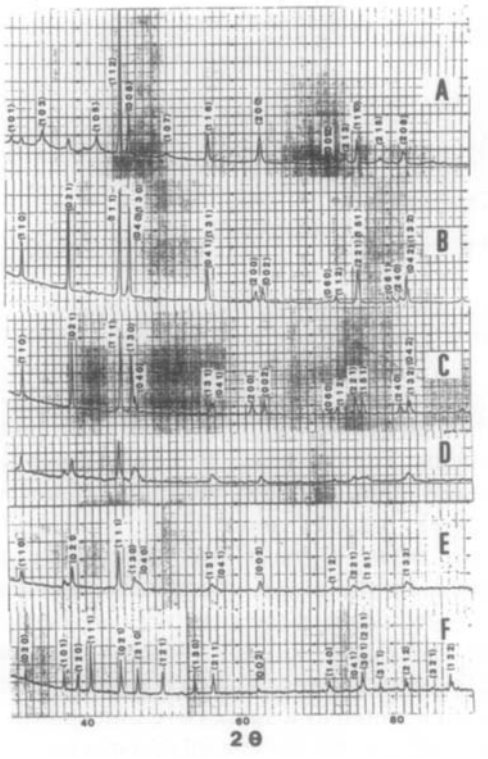

FIG. 4. Examples of X-ray powder patterns (Cu$K\alpha$ radiation).

	Composition	Annealing temperature (°C)	Indexing	Remarks
A	CrB	1040	MoB type	Unindexed lines correspond to the CrB type (MoB + CrB)
B	CrB	1200	CrB type	Pure CrB type
C	$Cr_{0.5}Mn_{0.5}B$	1200	CrB type	Pure CrB type
D	$Cr_{0.9}Mn_{0.9}B$	900	The same with E	(LTM)FeB + CrB type (see Fig. 5)
E	MnB	820	CrB type	The same with D
F	MnB	1200	FeB type	Pure FeB type (normal)

The CrB and MoB Type Phase

The X-ray powder diffraction pattern of the specimen with composition CrB annealed at 1040°C for 15 days after reaction at 850°C for 10 days is shown in Fig. 4A. This pattern is indexed as a mixture of tetragonal MoB and orthorhombic CrB type. Diffuse line shape for lines indexed (hkl) with odd numbers l of the MoB type such as (103), (105) implies imperfect ordering of the CrB type stucture layers in the MoB type structure, which may be like that seen in WB (*17*). This type of powder pattern was obtained in specimens annealed up to 1120°C. At higher temperatures, this structure irreversibly converts to the CrB type structure. However it is not clear whether both structures coexist at a temperature lower than 1120°C in the equilibrium state; further annealing at the same temperature did not give a significant difference in the X-ray patterns.

In the system $Cr_xMn_{1-x}B$, the transition temperature decreases with decreasing x. This may be concerned with deviation of the trigonal prism face from square in the CrB type structure, however the face of the trigonal prism must be square to form the MoB type structure. The dimension of the prism face sides is 0.2965 nm perpendicular

to the zigzag chain of borons and 0.2931 nm parallel to it, and the shape is very close to square. Both sides are distorted equally to 0.2949 nm in the MoB type. Substituting manganese for half of the chromium elongates the a axis lattice parameter of the CrB type unit cell to 0.2999 nm while the c axis remains unchanged at 0.2931 nm.

The FeB Type Phase

The FeB type structure emerges in specimens with manganese content above 10 at%. The X-ray powder pattern of melted $Cr_{0.85}Mn_{0.15}B$ indicated coexistence of the CrB and the FeB type structures. The single phase of the FeB type structure without the CrB type was obtained at compositions above 20 at% manganese. The transition temperature from the CrB to the FeB type decreases with increasing manganese content. The conversion is reversible, though that from FeB to CrB is sluggish. For example, the $Cr_{0.8}Mn_{0.2}B$ with the FeB type structure annealed at 1200°C for 2 days underwent transformation to the CrB type but some detectable amount of the FeB type structure still remained.

The Low-Temperature Modification of the FeB Type

At temperatures lower than about 1050°C, there appears another kind of structure in the composition range near MnB. The X-ray powder pattern is shown in Fig. 4D and E. This diffraction pattern consists of two sets of diffraction patterns. One is that of the CrB type and the other is that of the low-temperature modification of the FeB type, which is hereafter referred to as (LTM)FeB. The diffraction pattern of (LTM)FeB is very similar to that of the normal FeB type, but shows extinction of some lines as shown in Fig. 5. This (LTM)FeB can be obtained only in a narrow temperature range for the composition FeB. It converts to the higher temperature, normal modification FeB type structure at about 740°C irreversibly. Samples with the composition FeB annealed below 650°C gave an X-ray diffraction pattern of the Fe_2B type structure, in spite of the existence of excess boron atoms for composition Fe_2B. These samples also converted to the normal FeB type irreversibly above 740°C.

The concept of unit-cell twinning of close-packed structures makes it easy to understand the geometrical relation between the CrB and the FeB type structure. For convenience, the orthohexagonal unit cell is adopted to denote the structures. Projections along b_{oh} (the b axis of the orthohexagonal unit cell) of the hexagonal and the cubic close-packed structures are presented in Fig. 6 (*13*). The conventional Jagodzinski–Wykoff notation is used to denote the stackings of the layers. The letters h and c mean hexagonal- and cubic-like stackings of close-packed layers and the subscript means the number of layers in the unit cell. Dotted lines in Fig. 6 indicate traces of the twinning planes to form the trigonal prismatic holes, the center of which are occupied by boron atoms. The FeB and CrB type structures are formed from $(h)_2$ and $(c)_3$, respectively, by unit cell twinning of (1.1) (*18*). A drawing of the structures projected perpendicular to the twinned plane is presented in Fig. 3. Here, both the structures can be regarded as stacking variants of the other.

Similarities of X-ray powder patterns between (LTM)FeB and normal FeB type imply that the basic structure does not change between these structures.

Parthe and collaborators (*1, 4, 14–16*) have extensively investigated MSi, MGe, and MNi compounds with the CrB or the FeB type structures (where M is a rare earth metal). The following two points are interesting:

(i) DySi, HoSi, ErSi, and PrGe show polymorphism, i.e., low-temperature form

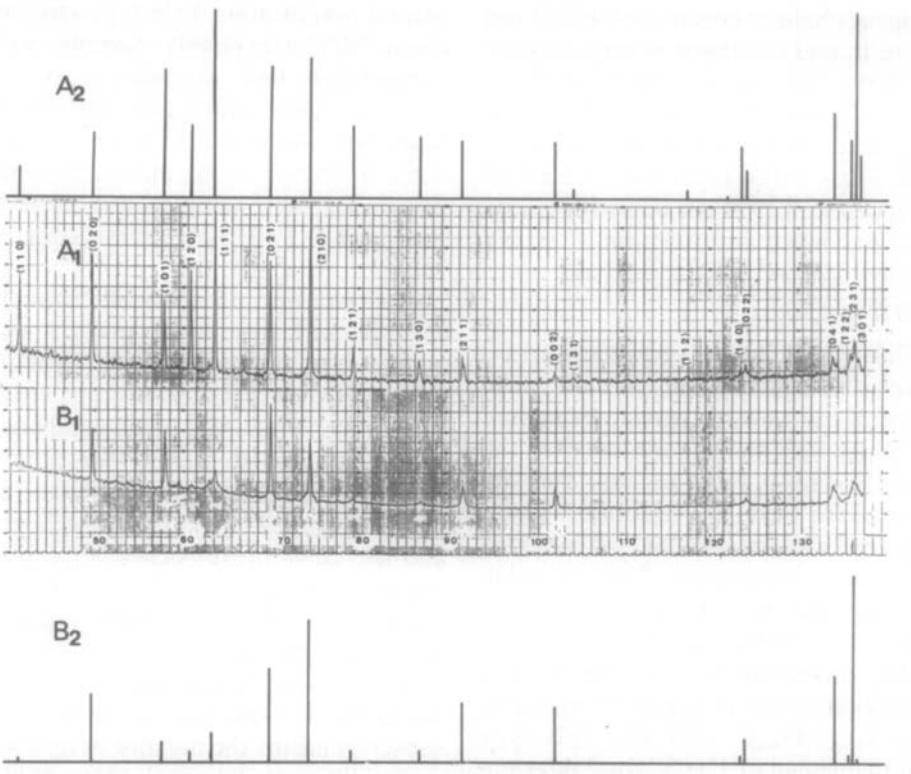

FIG. 5. Calculated and observed X-ray powder patterns of the normal FeB and (LTM)FeB (Cr$K\alpha$ radiation). A_1, normal FeB (observed); A_2, calculated with $P_A = 1.00$; B_1, (LTM)FeB (observed); B_2, calculated with $P_A = 0.55$, $P_B = P_C = P_D = 0.15$. This powder pattern is qualitatively in good agreement with the observed one.

with CrB type structure and high-temperature form with FeB type structure.

(ii) In the pseudobinary systems GdNi–YNi and GdNi–DyNi, phases with ordered stackings of the FeB and the CrB types have been found. Moreover, TbNi crystallizes in two structure types of the ordered intergrowth of the FeB and the CrB type structures, i.e. $(hhhhcc)_3$ at low temperature and $(hcc)_2$ at high temperature. It is to be noted that GdNi has the CrB type, DyNi and YNi the FeB type structure, and TbNi is between GdNi(CrB-type) and DyNi(FeB-type).

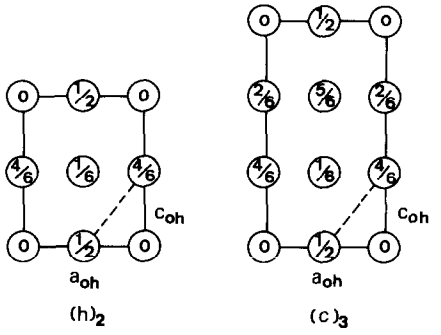

FIG. 6. Hexagonal $(h)_2$ and cubic $(c)_3$ close-packed structures described with orthohexagonal unit cells along b_{oh} (//). Traces of twinning planes are indicated by dotted lines.

In the CrB–MnB system, the low-temperature CrB type transforms to a high-temperature FeB type structure. This is very similar phenomenologically to (i). To the author's knowledge, no papers have been published on compounds with random stacking of CrB and FeB type structures.

TABLE I

MAGNETIC PROPERTIES OF THE NORMAL FeB AND THE (LTM)FeB

	Ferromagnetic Curie temperature (K)	Bohr magneton values per iron atom (μ_B) at 4 K	Internal magnetic field (kOe) at 300 K
Normal FeB	602	1.09	124
(LTM) FeB	602	1.09	108

From the viewpoint of thermodynamics, it is hardly acceptable that the (LTM)FeB appearing at the composition FeB and near MnB is in chemical equilibrium. Taking the experimental facts (ii) into consideration, the (LTM)FeB structure must be the ordered intergrowth of the FeB and CrB type structures in chemical equilibrium. Due to the slow diffusion rate below about 1000°C, however, the disordered intergrowth structures appear as a nonequilibrium state.

From the viewpoint of physical properties, especially magnetic properties, both phases are very similar to each other as is shown in Table I. Fruchart (*12*) proposed a model structure of the (LTM)FeB in which he suggested a defect arrangement for the (LTM)FeB with an exchange of atomic positions between an iron atom and a pair of boron atoms in adjacent triangular prisms. This exchange of boron and iron atoms would lead to metal–metal distances less than the separation in pure iron metal and also to breakup of the boron chains, which has to strongly affect the magnetic properties, as pointed out by DeYoung *et al.* (*19*). This is at variance with the experimental facts of the magnetic properties as shown above. It is also hardly probable that this model is able to explain the absence of several diffraction lines present in normal FeB (cf. Fig. 5).

Here the present author would like to propose a new model structure for the (LTM)FeB based on the random stacking of CrB and FeB type structures.

Now let us calculate the intensity of the X-ray powder diffraction patterns of this model structure.

Generally the diffracted X-ray intensity, when the crystal has an irregular lattice, is expressed (*20*) as

$$I \propto \sum_n \sum_{n'} Fn Fn'^* \exp\{-2\pi i \mathbf{b}(\mathbf{R}n - \mathbf{R}n')\}$$

where Fn is a form factor of the nth unit cell, Fn^* is that of the conjugate, $\mathbf{b}$ is the scattering vector, and $\mathbf{R}n$ is the positional vector of the nth unit cell. When the irregularity of the crystal consists of irregular layers, the equation mentioned above can be rewritten as follows (*21*):

$$I(\xi\,\eta\,\zeta) \propto \sum_{m=-(N-1)}^{N-1} (N - m) Jm(\xi\,\eta\,\zeta) \exp(-im\phi)$$

where

$$Jm(\xi\,\eta\,\zeta) = \langle Vs(\xi\,\eta\,\zeta, p) Vs^*(\xi\,\eta\,\zeta, p + m)\rangle_p$$

$$\phi = 2\pi\zeta$$

$$Vs(\xi\,\eta\,\zeta) = \frac{\sin L\pi\xi}{\sin \pi\xi} \frac{\sin M\pi\eta}{\sin \pi\eta} Fs(\xi\,\eta\,\zeta)$$

where L, M, and N, are the fractions along the a, b, and c axes of the crystal, Vs is the layer form factor which is taken for Fs as the Laue functions concerning ξ and η are multiplied to the whole of the equation, Jm is the average product of the layer form factors of the pth layer and the conjugate of the $(p + m)$th layer taken over the range p keeping m constant, i.e.

when

$$m \geq 0, \quad p = 1, 2, 3, \ldots, (N - m)$$

$$m < 0, \; p = |m| + 1, |m| + 2, \ldots, N.$$

Taking the existence probability and connecting probability of the layers into account, this equation can be expressed in a

more concrete form as follows

$$I(\xi\,\eta\,\zeta) \propto \sum_{m} (N - m) \times \left(\sum_{s=1}^{S} \sum_{t=1}^{S} A_{st}(m) V_s V_t^* \right) \exp(-im\phi)$$

where $A_{st}(m)$ is the probability that two layers distant m are s kind and t kind, and S is the number of species of the layers.

Four kinds of layer structures are adopted for the calculation, and these layer structures are shown in Fig. 7. These four kinds of structure are enough to construct any kind of mixed stacking variants of the FeB and the CrB type structures. For example, stackings of the same kind of layers along the b axis make the FeB type structure or $(h)_2$, alternative A and D or B and C stackings make CrB or $(c)_3$, and A,B,A,A,D,C,A, . . . make *hchchhcchcch* . . . .

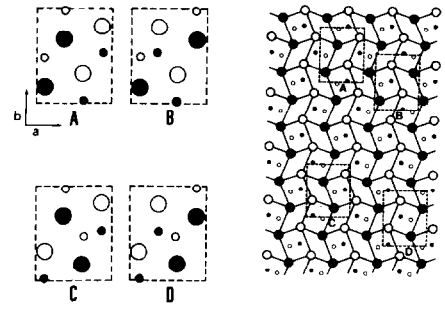

FIG. 7. Four types of layer structures. Small circles and large circles represent boron atoms and metal atoms, respectively; open and closed circles are at height of ¼ and ¾. These four types of layer unit cells can be observed in the normal structure as shown in the right figure, and stacking of these layers along the b axis makes various kinds of stacking variants.

TABLE II

INTENSITY CALCULATION FOR MIXED STACKING VARIANTS OF FeB[a]

			I/I_0(calculated) when P_A =						I_{obs}		
hkl	*d*(nm)	2θ (deg.)	1.00	0.85	0.70	0.55	0.40	0.25	0.10	Normal	(LTM)
1 1 0	0.3265	41.05	16.04	10.54	5.93	2.65	0.68	0.02	0.68	s	w
0 2 0	0.2750	49.20	35.99	36.91	36.86	36.86	36.91	37.01	37.17	vs	vs
1 0 0	0.2384	57.39	67.67	44.44	25.00	11.15	2.85	0.07	2.87	s	s
1 2 0	0.2276	60.38	38.28	25.14	14.14	6.31	1.61	0.04	1.62	vs	w
1 1 1	0.2188	63.11	100.00	65.67	36.93	16.47	4.20	0.11	4.23	vs	m
0 2 1	0.2011	69.42	69.16	70.92	70.82	70.82	70.92	71.12	71.42	s	s
2 1 0	0.1903	73.94	73.53	75.69	75.72	75.72	75.69	75.61	75.51	vs	vs
1 2 1	0.1801	78.91	38.20	25.08	14.11	6.29	1.60	0.04	1.61	m	w
1 3 0	0.1671	86.50	32.74	21.50	12.09	5.39	1.37	0.03	1.38	m	w
2 1 1	0.1599	91.45	30.40	31.12	31.05	31.05	31.12	31.26	31.43	m	m
0 0 2	0.1473	101.98	29.16	29.90	29.86	29.86	29.90	29.99	30.12	m	m
1 3 1	0.1453	103.94	5.24	3.44	1.93	0.86	0.22	0.01	0.22	w	—
2 3 0	0.1360	114.62	1.34	1.35	1.34	1.34	1.35	1.37	1.41	—	—
1 1 2	0.1343	116.96	4.23	2.81	1.58	0.71	0.18	0.01	0.18	w	—
3 1 0	0.1313	121.29	2.98	1.96	1.10	0.49	0.13	0.00	0.13	—	—
1 4 0	0.1302	123.06	29.19	19.17	10.78	4.81	1.23	0.03	1.23	m	—
0 2 2	0.1299	123.65	14.42	14.79	14.77	14.77	14.79	14.83	14.89	m	m
0 4 1	0.1246	133.49	46.11	47.28	47.22	47.22	47.28	47.42	47.62	s	s
1 2 2	0.1237	135.50	31.87	20.93	11.77	5.25	1.34	0.03	1.35	m	w
2 3 1	0.1235	135.93	97.24	100.00	100.00	100.00	100.00	100.00	100.00	s	s
3 0 1	0.1229	137.28	23.22	15.25	8.58	3.83	0.98	0.03	0.98	m	w

[a] Dimensions of the basic unit cell: a = 0.40577 nm, b = 0.5495 nm, c = 0.29467 nm; Cr$K\alpha$ radiation.

Two of the boron atom position in a unit cell can be determined independently of the stackings, but another two of them depend on the method of stacking. So the probability of the boron positions are taken into account relative to the stackings.

Taking the existence probability of each layer as a variable, the intensity of the powder pattern was calculated. The result is presented in Table II. For example, in the case of the existence probability of A layers P_A being 0.7, those of B, C, and D layers (P_B, P_C, and P_D) were assumed to be equal at 0.1 for convenience. This result clearly shows that the intensities for the diffraction lines (hkl) with $h = 2n + 1$ decrease with decreasing P_A, i.e., the portion of hexagonal close-packed layers. However, the decrease of P_A does not always correspond to an increase of the portion of cubic-like layers especially in the region where P_A has small values.

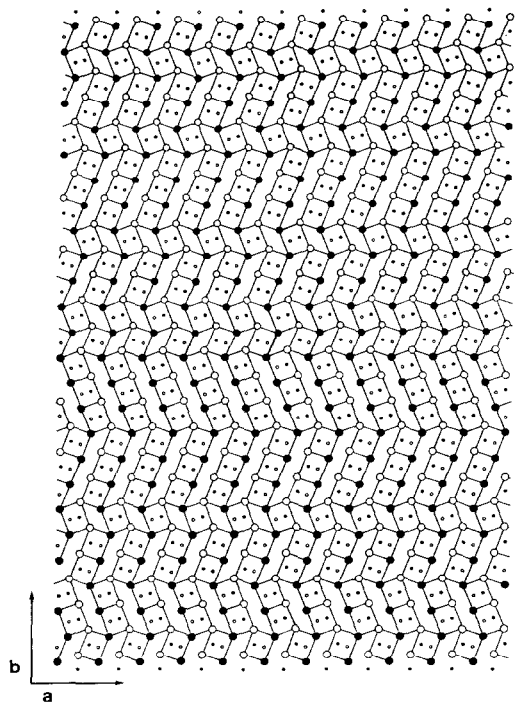

FIG. 8. Proposed model structure for the (LTM)FeB. This model was simulated with $P_A = 0.55$ and $P_B = P_C = P_D = 0.15$. This structure can explain the observed X-ray diffraction patterns of the (LTM)FeB as a whole, as shown in Fig. $5B_2$.

As a whole, the observed powder pattern for (LTM)FeB is in good agreement with the calculated one for $P_A = 0.55$, as shown in Fig. $5B_1$ and B_2. The model structure with $P_A = 0.55$ is shown in Fig. 8.

It is to be noted in Table II and Fig. 5B that the observed intensity of (101) is stronger than the calculated value. At present, the author has no explanation for this.

Mössbauer effect measurements on both the normal FeB and the (LTM)FeB (*22*) give interesting information concerning the crystal structures. The Mössbauer spectrum of normal FeB has six clearly split lines of ferromagnetic ^{57}Fe, indicating that the iron site is one kind, while the spectrum of (LTM)FeB has six broad lines of somewhat smaller internal magnetic field indicating existence of different kinds of iron sites. The present author explains these broad spectrum lines and smaller effective internal field in terms of an anisotropic hyperfine field and fluctuation of the iron sites in local symmetry in the (LTM)FeB (*22*). This interpretation is not in conflict with the proposed structure model. Thus we can understand the magnetic properties of (LTM)FeB compared with normal FeB by this model. In this model, the atomic distances (Me-Me, B–B, and Me–B) and coordination numbers are unchanged, but only the local symmetry is changed between h and c layers.

Acknowledgments

The author wishes to express his cordial thanks to Professor S. Kachi for valuable discussion and continual encouragement. And many useful discussions with Professor K. Kosuge, who also revised the manuscript of this article, is gratefully acknowledged. He is much indebted to Professor M. Shimada for useful suggestions about high pressure techniques.

References

1. D. HOHNKE AND E. PARTHE, *Acta Crystallogr.* **20,** 572 (1966).
2. A. E. DWIGHT, R. A. CONNER, JR., AND J. W. DOWNEY, *Acta Crystallogr.* **18,** 835 (1965).
3. R. LEMAIRE AND D. PACCARD, *J. Less-Common Met.* **21,** 403 (1970).
4. K. KLEPP AND E. PARTHE, *Acta Crystallogr.* **B36,** 774 (1980).
5. F. MERLO AND M. L. FORNASINI, *Acta Crystallogr.* **B37,** 500 (1981).
6. A. WITTMANN, H. NOWOTNY, AND H. BOLLER, *Mh. Chem.* **91,** 608 (1960).
7. S. ANDERSSON AND B. G. HYDE, *J. Solid State Chem.* **9,** 92 (1974).
8. B. G. HYDE, A. N. BAGSHAW, S. ANDERSSON, AND M. O'KEEFFE, *Annu. Rev. Bater. Sci.* **4,** 43 (1974).
9. M. C. CADEVILLE AND E. DANIEL, *J. Phys. (Paris)* **27,** 449 (1966).
10. N. LUNDQUIST AND H. P. MYERS, *Ark. Fys.* **20,** 463 (1961).
11. T. SHIGEMATSU, T. KANAIZUKA, K. KOSUGE, M. SHIGA, Y. NAKAMURA, AND S. KACHI, *Phys. Lett.* **53A,** 385 (1975).
12. T. SHIGEMATSU, T. KANAIZUKA, AND S. KACHI, *J. Inst. Met.* **40,** 1131 (1976) (in Japanese).
13. R. FRUCHART, *Ann. Chem.* **4,** 1247 (1959).
14. E. PARTHE, *Acta Crystallogr.* **B32,** 2813 (1976).
15. J. ROY, J. M. MOREAN, D. PACCARD, AND E. PARTHE, *Acta Crystallogr.* **B34,** 9 (1978).
16. K. KLEPP AND E. PARTHE, *Acta Crystallogr.* **B37,** 495 (1981).
17. H. BOLLER, W. RIEGER, AND H. NOWOTNY, *Mh. Chem.* **95,** 1497 (1964).
18. B. G. HYDE, S. ANDERSSON, M. BAKKER, C. H. PLUG, AND M. O'KEEFFE, *Prog. Solid State Chem.* **12,** 273 (1977).
19. D. B. DEYOUNG AND R. G. BARNES, *J. Chem. Phys.* **62,** 1726 (1974).
20. A. J. C. WILSON, *Proc. Roy. Soc.* **A180,** 277 (1942).
21. I. NITTA, "X-ray Crystallography (in Japanese), Maruzen, Tokyo (1959).
22. T. KANAIZUKA, *Phys. Status Solidi,* submitted.